

Manipulation of non-linear heat currents in the dissipative Anderson-Holstein model

Bitan De and Bhaskaran Muralidharan*

Department of Electrical Engineering, Indian Institute of Technology Bombay, Powai, Mumbai-400076, India

(Dated: March 12, 2022)

The anomalous behavior of electron induced phonon transport is investigated using an *Anderson-Holstein* based dissipative quantum dot setup under two relevant bias situations: (a) a voltage bias in the absence of an electronic temperature gradient and (b) an electronic temperature gradient at zero voltage. It is shown that the direction of phonon transport in the non-linear regime is different in the two cases since the first case facilitates the accumulation of phonons in the dot and the second case leads to the absorption of phonons in the dot. In the linear regime, both the phonon and electronic transport get decoupled and Onsager's symmetry is verified. We explain the observed cumulative effects of voltage and electronic temperature gradients on the non-linear phonon currents by introducing a new transport coefficient that we term as the *electron induced phonon thermal conductivity*. It is demonstrated that under suitable operating conditions in Case (a) the dot can pump in phonons into the hotter phonon reservoirs and in Case (b) the dot can extract phonons out of the colder phonon reservoirs. Finally, we elaborate on how the non-linear electronic heat current can be stimulated and controlled by engineering the temperature of the phonon reservoirs even under vanishing effective electron flow.

I. INTRODUCTION

The physics of electron-phonon interaction has gained significant interest¹ with its fingerprints being captured in diverse physical systems like superconductors²⁻⁶, cavity-coupled mesoscopic conductors^{7,8}, optomechanical systems^{9,10} and electronic devices^{11,12}, to name a few. So far, the research in this area is primarily carried out along two predominant directions: (a) exploration of novel experimental techniques to detect such interactions¹³⁻¹⁷ and (b) theoretical studies on the effect of electron-phonon coupling on quantum phenomena in the nanoscale¹⁸⁻²⁷. Typically in microscopic thermoelectric setups, the former direction concerns materials synthesis, device fabrication and the integration at the systems level^{28,29}. The principal goal in this case, is to control the flow of waste heat to optimize the efficiency of energy conversion³⁰⁻³³. On the other hand, the latter direction deals with the dynamics of charge and heat transport from a quantum transport perspective. From the application point of view, this approach aims to propose new devices to realize novel paradigms like *phonon computation*³⁴⁻³⁸.

Many notable works have established that in the zero-dimensional systems such as quantum dots,³⁹⁻⁴¹ the interplay of electrons and phonons gives rise to some unique features manifesting as transport signatures⁴²⁻⁴⁶. Here, typical to quantum transport set ups, electronic and phonon currents are driven by applying a bias voltage and/or a thermal bias across the contacts. While voltage induced phonon transport has been the subject of many theoretical works⁴⁷⁻⁵², understanding the non-equilibrium phonon transport under an electronic temperature bias has not been explored so far, which will be the objective of this paper.

Our objective in this work is to compare the nature of the electronically stimulated phonon transport in two cases via: Case (a): a voltage bias in the absence of an

electronic temperature bias and Case (b): an electronic temperature bias at zero voltage. It is shown by the simulation framework that the polarity of phonon current in the nonlinear regime is opposite in the two cases since the first case facilitates the accumulation of phonons in the dot and the second case leads to the absorption of phonons in the dot.

In Case (a), surplus phonons heat up the dot and are suitably extracted by the phonon reservoirs kept in equilibrium. In Case (b), the dot cools down for being phonon deficient and the reservoirs pump in phonons into it. However in the linear regime, phonon and electron transport get decoupled and Onsager's reciprocity is verified.

In our previous work⁵³, we explored the *non-linear phonon Peltier effect* by noticing the voltage dependence of the non-linear phonon current. In the current work, we propose a new parameter called, *electron-assisted phonon thermal conductivity* to signify the mutual dependence of phonon currents on the voltage and electronic temperature gradient.

We also notice that the polarity of phonon transport can be controlled by differing the temperature of phonon reservoirs from the temperature of electronic contacts. In Case (a), phonons flow from the reservoirs to the dot at low voltage when the reservoirs are hotter than the contacts. At large voltage, the polarity of phonon flow is reversed and the phonons are pumped into the hotter reservoirs. An opposite situation is observed in Case (b) given the reservoirs are colder than the contacts. In this case, phonons relax from the dot to the reservoirs at low electronic temperature gradient. When the temperature gradient is large, the direction of phonon flow is reversed and phonons are extracted from the colder reservoirs. In both cases, the direction of phonon current is verified by estimating the dot temperature with a phonon thermometer bath weakly coupled to the dot. Finally, we elaborate on how the non-linear electronic heat current can be stimulated and controlled by engineering

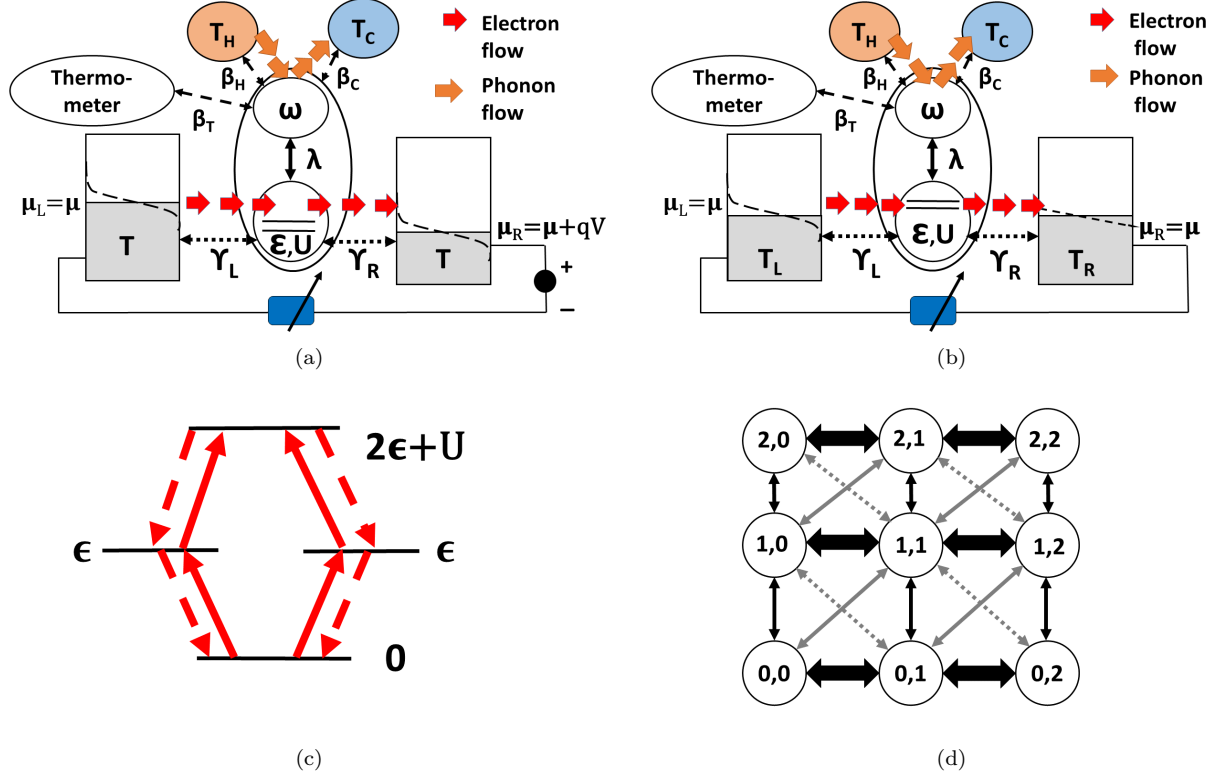


Figure 1. Non-equilibrium charge current (shown in red bold arrow) is driven through the central dot in two ways: either by applying (a) voltage bias or (b) by applying electronic temperature gradient across the contacts L and R . Dot phonon current (shown by orange bold arrows) is set up by creating a thermal gradient across the reservoirs H and C . In both (a) and (b) the dot temperature is monitored by *phonon thermometer* bath. (c) The state transition diagram in the electronic Fock space. (d) The state transition diagram in the many body electron-phonon Fock space. Direct electron tunnelings (depicted by thin black double arrows) occur between states $|n, q\rangle$ and $|n \pm 1, q\rangle$, while phonon assisted electron tunnelings (depicted by gray thin double arrows) happen between states $|n, q\rangle$ and $|n \pm 1, q'\rangle$. Reservoir assisted phonon transitions (represented by black bold arrows) take place between the states $|n, q\rangle$ and $|n, q \pm 1\rangle$.

the temperature of the phonon reservoirs even under vanishing effective electron flow.

This paper is organized as follows: Section II introduces the device model and formulates the transport equations. In the Sec. III A, we focus on the comparative study of the characteristics of the phonon currents in the two cases under consideration. Section III B introduces the electron assisted phonon thermal conductivity coefficient and compares it with the conventional electronic thermal conductivity. In the Sec. III C, we describe the engineering of the temperature of the phonon reservoirs to modulate the flow of the phonon and electronic heat currents. In the Sec. IV, we summarize our results and conclude.

II. PHYSICS AND FORMULATION

The schematics of the set ups to be studied here are depicted in Fig.1(a) and Fig.1(b). Each of them typically comprises a single quantum dot weakly coupled to the

electronic contacts α_1 ($\alpha_1 \in L, R$), and the phonon reservoirs α_2 ($\alpha_2 \in H, C$). The dot is described by the dissipative *Anderson-Holestein* model which has both electronic and phonon degrees of freedom interacting with each other. The electronic current is driven through the device in two ways: Case (i): by applying a voltage bias (shown in Fig.1(a)) across the contacts L and R and Case (ii) by applying an electronic temperature gradient (shown in Fig.1(b)) across the contacts L and R . The phonon current is set up by applying a thermal bias across the phonon reservoirs H and C . In addition, the electron current gives rise to a phonon current even in the absence of a temperature bias across the reservoirs H and C , provided the electron-phonon coupling is finite. The direction of phonon flow depends on the dot temperature (T_M), which is estimated by a phonon thermometer bath weakly coupled to the dot.

1. Model Hamiltonian

The composite system Hamiltonian \hat{H} can be written as $\hat{H} = \hat{H}_D + \hat{H}_{\alpha_1} + \hat{H}_{\alpha_2} + \hat{H}_{\alpha_1 D} + \hat{H}_{\alpha_2 D}$. Here \hat{H}_D , \hat{H}_{α_1} , \hat{H}_{α_2} denote the respective Hamiltonians of the dot, the contacts and the reservoirs, while $\hat{H}_{\alpha_1 D}$ and $\hat{H}_{\alpha_2 D}$ represent the dot-to-contact electronic tunneling processes and the dot-to-reservoir phonon relaxation processes respectively. The dot Hamiltonian is further divided as,

$$\hat{H}_D = \hat{H}_{el} + \hat{H}_{ph} + \hat{H}_{el-ph}. \quad (1)$$

The electronic part (\hat{H}_{el}) consists of a single spin degenerate energy level with an on-site energy ϵ and a Coulomb interaction energy U for double occupancy. The phonon part (\hat{H}_{ph}) comprises of a single phonon mode ν with angular frequency ω_ν . Inside the dot, the electrons and phonons interact through a dimensionless parameter λ_ν . Hence, H_{el} , H_{ph} , H_{el-ph} are given by,

$$\begin{aligned} \hat{H}_{el} &= \left(\sum_{\sigma} \epsilon d_{\sigma}^{\dagger} d_{\sigma} + U d_{\uparrow}^{\dagger} d_{\uparrow} d_{\downarrow}^{\dagger} d_{\downarrow} \right), \\ \hat{H}_{ph} &= \hbar \omega_{\nu} \hat{b}_{\nu}^{\dagger} \hat{b}_{\nu}, \\ \hat{H}_{el-ph} &= \sum_{\sigma} \lambda_{\nu} \hbar \omega_{\nu} d_{\sigma}^{\dagger} d_{\sigma} (\hat{b}_{\nu}^{\dagger} + \hat{b}_{\nu}). \end{aligned} \quad (2)$$

In the above expressions, $d_{\sigma}^{\dagger} (d_{\sigma})$ and $b_{\nu}^{\dagger} (b_{\nu})$ are the respective creation(annihilation) operators of the electrons and phonons. The electronic contacts α_1 characterize a macroscopic body of non-interacting electrons in the momentum eigen state $\alpha_1 k$ and spin σ' with energies $\epsilon_{\alpha_1 k \sigma'}$. Similarly, the phonon reservoirs α_2 comprise of numerous phonon modes $\alpha_2 r$ with an angular frequency $\omega_{\alpha_2 r}$. They are defined by the following Hamiltonians,

$$\begin{aligned} \hat{H}_{\alpha_1} &= \sum_{\alpha_1 \in L, R} \sum_{\alpha_1 k \sigma'} \hat{c}_{\alpha_1 k \sigma'}^{\dagger} \hat{c}_{\alpha_1 k \sigma'}, \\ \hat{H}_{\alpha_2} &= \sum_{\alpha_2 \in H, C} \sum_{\alpha_2} \hat{B}_{\alpha_2 r}^{\dagger} \hat{B}_{\alpha_2 r}, \end{aligned} \quad (3)$$

where $\hat{c}_{\alpha_1 k \sigma'}^{\dagger} (\hat{c}_{\alpha_1 k \sigma'})$ creates (annihilates) an electron with momentum k and spin σ' in the contact α_1 , and $\hat{B}_{\alpha_2 r}^{\dagger} (\hat{B}_{\alpha_2 r})$ creates (annihilates) a phonon of angular frequency $\omega_{\alpha_2 r}$ in the reservoir α_2 . If the electrons in the dot are coupled to the electrons in the contacts α_1 through an energy $\tau_{\alpha_1 k \sigma' \sigma}^{el}$ and the phonons in the dot are coupled to the phonons in the reservoirs α_2 through an energy $\tau_{\alpha_2 r \nu}^{ph}$ then the coupling Hamiltonians $\hat{H}_{\alpha_1 D}$ and $\hat{H}_{\alpha_2 D}$ are given as follows

$$\begin{aligned} \hat{H}_{\alpha_1 D} &= \sum_{k \sigma' \sigma} [\tau_{\alpha_1 k \sigma' \sigma}^{el} \hat{c}_{\alpha_1 k \sigma'}^{\dagger} \hat{d}_{\sigma} + H.c], \\ \hat{H}_{\alpha_2 D} &= \sum_{\nu, \alpha_2} \tau_{\alpha_2 r \nu}^{ph} (\hat{B}_{\alpha_2 r}^{\dagger} + \hat{B}_{\alpha_2 r}) (\hat{b}_{\nu}^{\dagger} + \hat{b}_{\nu}). \end{aligned} \quad (4)$$

In this work, we assume that the phonon transition processes are mode independent and the electron tunneling processes are momentum conserved and spin independent. With this approximation we can rewrite $\tau_{\alpha_1 k \sigma' \sigma}^{el}$ and $\tau_{\alpha_2 r \nu}^{ph}$ simply as τ^{el} and τ^{ph} respectively.

The dot Hamiltonian is diagonalized by the polaron transformation (such that $\hat{H}_D \rightarrow \tilde{\hat{H}}_D = e^S \hat{H}_D e^{-S}$, where $S = \sum_{\nu} \lambda_{\nu} [\hat{b}_{\nu} - \hat{b}_{\nu}^{\dagger}]$). It transforms the dot fermionic operators $\hat{d}_{\sigma}^{\dagger} (\hat{d}_{\sigma})$ and leads to the renormalization of ϵ and U , such that $\tilde{\epsilon} = \epsilon - \lambda_{\nu}^2 \hbar \omega_{\nu}$ and $\tilde{U} = U - 2 \lambda_{\nu}^2 \hbar \omega_{\nu}$. The eigen states of $\tilde{\hat{H}}_D$ are represented by $|n, q\rangle$, where n and q are the electron and phonon number of the eigen states. The energy eigen values of those states become $E_{(n, q)} = \tilde{E}_n + q \hbar \omega_{\nu}$, where, $\tilde{E}_0 = 0, \tilde{E}_1 = \tilde{\epsilon}, \tilde{E}_2 = 2\tilde{\epsilon} + \tilde{U}$, corresponding to the $n = 0, 1$ and 2 electron number spaces respectively. This transformation also renormalizes the electronic tunneling energy τ^{el} , such that $\tilde{\tau}^{el} = \tau^{el} \exp[-\lambda_{\nu} (\hat{b}_{\nu} - \hat{b}_{\nu}^{\dagger})]$. However, the phonon coupling energy τ^{ph} is left unaltered due to the polaron transformation since the operator S commutes with the phonon operators $b_{\nu}^{\dagger} (b_{\nu})$ of the dot.

With the derived expressions of $\tilde{\tau}_{el}$ and τ_{ph} , we can evaluate the dot-to-contact electron tunneling rate γ_{α_1} and the dot-to-phonon relaxation rate β_{α_2} using the Fermi's golden rule. They are represented as: $\gamma_{\alpha_1} = \frac{2\pi}{\hbar} \sum_{\alpha_1} |\tilde{\tau}_{\alpha_1}^{el}|^2 \rho_{\alpha_1 \sigma'}$ and $\beta_{\alpha_2} = \frac{2\pi}{\hbar} \sum_{\alpha_2} |\tau_{\alpha_2}^{ph}|^2 D_{\alpha_2}$, where $\rho_{\alpha_1 \sigma'}$ and D_{α_2} are the constant electron and phonon density of states associated with the contacts α_1 and the reservoirs α_2 respectively. The study of the model Hamiltonian enables us to formulate the transport methodology, which we will analyze in the next subsection.

2. Transport methodology

Before we start the formulation of transport equations, it is imperative to explain the important approximations we have considered in this work. First, we set the rate of dot-to-reservoir phonon relaxation processes much lower than the rate of dot-to-contact electron tunneling processes ($\hbar \gamma_{\alpha_1} \gg \hbar \beta_{\alpha_2}$) to rule out the system damping⁵⁴. In this limit, the phonon currents emanating from the terminal phonon reservoirs remain uncorrelated and hence can be computed independently⁵⁵⁻⁵⁷. Second, we set $\hbar \gamma_{\alpha_1}, \hbar \beta_{\alpha_2} \ll k_B T$, so that the transport of the electrons and phonons through a single quantum dot weakly coupled to the electronic contacts and the phonon reservoirs can be described in the sequential tunneling regime in which charge and phonon currents are calculated via the quantum Master equation⁵⁸⁻⁶². Last, we neglect the overlap of the adjacent phonon sidebands, by setting the energy gap between the sidebands larger than the tunneling induced broadening of energy levels ($\hbar \omega_{\nu} \gg \hbar \gamma_{\alpha_1}$)⁶³. With this assumption, the Markov approximation is justified and two consecutive electron tunneling processes are completely uncorrelated since the memory of macro-

scopic contacts and reservoirs is negligible⁶⁴. Hence, the diagonal terms of the system density matrix get decoupled from the off-diagonal terms and the Master equation reduces to the rate equation^{65–67}.

The tunneling rate between two eigen states $|n, q\rangle$ and $|n \pm 1, q'\rangle$ is determined by the contact Fermi function of the energy difference of the two states and it is given by:

$$R_{(n,q) \rightarrow (n+1,q')} = \sum_{\alpha_1 \in L, R} \gamma_{\alpha_1} |\langle n, q | \hat{d}_\sigma | n+1, q' \rangle|^2 \times f_{\alpha_1}(E_{n+1,q'} - E_{n,q}), \quad (5)$$

$$R_{(n,q) \rightarrow (n-1,q')} = \sum_{\alpha_1 \in L, R} \gamma_{\alpha_1} |\langle n, q | \hat{d}_\sigma^\dagger | n-1, q' \rangle|^2 \times [1 - f_{\alpha_1}(E_{n,q} - E_{n-1,q'})], \quad (6)$$

where $f_{\alpha_1}(\zeta) = 1/(1 + \exp(\frac{\zeta - \mu_{\alpha_1}}{k_B T_{\alpha_1}}))$ is the Fermi-Dirac distribution function of the contact α_1 with chemical potential μ_{α_1} and temperature T_{α_1} . The phonon relaxation process between the reservoirs and the dot lead to the transition between two eigen states $|n, q\rangle$ and $|n, q \pm 1\rangle$ and the relaxation rate follows the Boltzmann ratio:

$$R_{(n,q) \rightarrow (n,q+1)} = \sum_{\alpha_2 \in H, C} \beta_{\alpha_2}(q+1) \exp\left(-\frac{\hbar\omega_\nu}{k_B T_{\alpha_2}}\right), \quad (7)$$

$$R_{(n,q) \rightarrow (n,q-1)} = \sum_{\alpha_2 \in H, C} \beta_{\alpha_2}(q+1). \quad (8)$$

Using the rate equations, the master equation for the probabilities $P_{(n,q)}$ of the many-body electron-phonon states $|n, q\rangle$ take the following form:

$$\begin{aligned} \frac{dP_{(n,q)}}{dt} = & \sum_{q'}^{N_q} \left[R_{(n',q') \rightarrow (n,q)}^{el} P_{(n',q')} - R_{(n,q) \rightarrow (n',q')}^{el} P_{(n,q)} \right] \\ & + \left[R_{(n',q') \rightarrow (n,q)}^{ph} P_{(n',q')} - R_{(n,q) \rightarrow (n',q')}^{ph} P_{(n,q)} \right] \delta(n \pm 1, n') \delta(q \pm 1, q'). \end{aligned} \quad (9)$$

In the steady state, the derivative in the left hand side of (9) vanishes and the steady state probabilities $P_{(n,q)}$ can be determined by solving the algebraic equations. We use the probabilities to compute the charge currents, the electronic heat currents associated with the contacts α_1 and the phonon heat currents associated with reservoirs α_2 . They are given as,

$$I_{\alpha_1} = \sum_{q=0}^{N_q} \sum_{q'=0}^{N_q} -q \left[R_{(n+1,q') \rightarrow (n,q)}^{el_{\alpha_1}} P_{(n+1,q')} - R_{(n+1,q') \rightarrow (n,q)}^{el_{\alpha_1}} P_{(n,q)} \right], \quad (10)$$

$$I_{el_{\alpha_1}}^Q = \sum_{q=0}^{N_q} \sum_{q'=0}^{N_q} (E_{n+1,q'} - E_{n,q} - \mu_\alpha) \left[R_{(n+1,q') \rightarrow (n,q)}^{el_{\alpha_1}} P_{(n+1,q')} - R_{(n+1,q') \rightarrow (n,q)}^{el_{\alpha_1}} P_{(n,q)} \right], \quad (11)$$

$$I_{ph_{\alpha_2}}^Q = \sum_{q=0}^{N_q} \sum_{q'=0}^{N_q} \hbar\omega_\nu \left[R_{(n,q) \rightarrow (n',q')}^{ph_{\alpha_2}} P_{(n,q)} - R_{(n',q') \rightarrow (n,q)}^{ph_{\alpha_2}} P_{(n',q')} \right] \delta(n, n') \delta(q \pm 1, q'). \quad (12)$$

Now it is evident from (5) and (6) that the transition between the states $|n, q\rangle$ and $|n \pm 1, q'\rangle$ leads to the net phonon generation (or absorption) in the dot. In the next subsection we will focus on the role of λ_ν in controlling the phonon generation (or absorption). Considering the law of charge conservation, in the rest of the paper we will denote $I_L = -I_R = I$.

3. Effect of interaction on phonon transport

The effective electron tunneling rate ($\gamma_{\alpha_1}^{eff}$) between the states $|n, q\rangle$ and $|n \pm 1, q'\rangle$ is modified by the *Frank-Condon* overlapping factor between the two states^{68–70}. The effective electron tunneling rate is given as

$$\gamma_{\alpha_1}^{eff} = \gamma_{\alpha_1} |FC_{q,q'}|^2 = \gamma_{\alpha_1} \left[|\langle n, q | \hat{d}^\dagger | n', q' \rangle|^2 \delta(n', n-1) + |\langle n, q | \hat{d} | n', q' \rangle|^2 \delta(n', n+1) \right], \quad (13)$$

where $|FC_{q,q'}|^2 = \exp(-\lambda_\nu^2) \frac{k!}{K!} \lambda_\nu^{2(K-k)} [L_k^{K-k}(\lambda_\nu^2)]^2$ is the *Frank-Condon* factor between the two states with phonon number q and q' and L_k^{K-k} is the associated Laguerre polynomial with $k = \min(q, q')$ and $K = \max(q, q')$. The net phonon generation (or absorption) in the dot due to the transition between the states $|n, q\rangle$ and $|n \pm 1, q'\rangle$, takes place at a rate²⁶

$$GE_{ph}^{\alpha_1} = \sum_{n,q} \sum_{n \pm 1} (q' - q) P_{n,q} R_{(n,q) \rightarrow (n \pm 1, q')}^{\alpha_1}, \quad (14)$$

It is evident that in the limit $\hbar\gamma_{\alpha_1} \gg \hbar\beta_{\alpha_2}$, the phonon distribution in the dot is primarily determined by the electron transport. When $q \neq q'$, the phonons generate (or get absorbed) in the dot and the average phonon number in the dot $\langle N_{ph} \rangle = \sum_{n,q} q P_{n,q}$ deviates from the equilibrium phonon distribution $\langle N_{ph}^{eq} \rangle$ of the phonon reservoirs. The excess phonons are extracted by the reservoirs at a

rate²⁶

$$\begin{aligned}
 RE_{ph}^{\alpha_2} &= \sum_{q=0}^{N_q} \sum_{q'=0}^{N_q} \hbar\omega_\nu \left[R_{(n,q) \rightarrow (n',q')}^{ph\alpha_2} P_{(n,q)} \right. \\
 &\quad \left. - R_{(n',q') \rightarrow (n,q)}^{ph\alpha_2} P_{(n',q')} \right] \delta(n, n') \delta(q \pm 1, q') \quad (15) \\
 RE_{ph}^{\alpha_2} &= \beta_{\alpha_2} \frac{\langle N_{ph} \rangle - \langle N_{ph} \rangle^{eq}}{1 + \langle N_{ph} \rangle^{eq}}.
 \end{aligned}$$

It is evident from (12) and (15) that the phonon current $I_{ph}^Q = \hbar\omega RE_{ph}^{\alpha_2}$. It is noticed from (13), that when $\lambda_\nu = 0$, $\gamma_{\alpha_1}^{eff}$ vanishes unless $q = q'$. In this case, $\langle N_{ph} \rangle$ equals with $\langle N_{ph}^{eq} \rangle$ and $I_{ph\alpha_2}^Q$ vanishes. On the other way, when λ_ν is non-zero, $\langle N_{ph} \rangle$ deviates from $\langle N_{ph}^{eq} \rangle$ and $I_{ph\alpha_2}^Q$ becomes finite. The deviation of $\langle N_{ph} \rangle$ from $\langle N_{ph}^{eq} \rangle$ causes the variation of dot temperature T_M from the equilibrium reservoir temperature T_{α_2} . The dot temperature can be computed from the Boltzmann ratio by with a quasi-equilibrium approximation²⁴ as:

$$T_M = \frac{\hbar\omega_\nu}{k_B} \left[\ln \left(\frac{P_{n,q}}{P_{n,q+1}} \right) \right]^{-1} \quad (16)$$

We will notice in the next section that the electron induced phonon current shows different characteristics depending on whether the electron flow is stimulated by a voltage bias or by an electronic temperature bias. From now on, we will denote λ_ν , ω_ν , $GE_{ph}^{\alpha_1}$ and $RE_{ph}^{\alpha_2}$ simply as λ , ω , G_{ph} and R_{ph} . Also, unless otherwise mentioned, the electronic contact coupling and reservoir phonon couplings are assumed to be symmetric (i.e $\gamma_{\alpha_1} = \gamma$, $\gamma_{\alpha_1}^{eff} = \gamma^{eff}$ and $\beta_{\alpha_2} = \beta$, where $\alpha_2 \in H, C$).

III. RESULTS

A. Electron-phonon coupled transport

In this section we focus on the electron-phonon coupled transport in our setup. Each operating point is signified by a voltage bias, an electronic temperature gradient ($\Delta T_{el} = T_L - T_R$) applied across the contacts and a phonon temperature gradient ($\Delta T_{ph} = T_H - T_C$) applied between the reservoirs. In our analysis, we set $(k_B T \gg \hbar\omega \gg \hbar\gamma, \hbar\beta)$ the tunnel induced broadening of the energy levels in the dot small to ensure that the levels do not overlap. Under this condition, transport is described in the sequential tunneling limit, where charge and heat current are calculated via rate equation. Additionally we assume the dot functions as n-type, i.e $\epsilon \gg \mu$.

First we demonstrate the effect of electron current on I_{ph}^Q in two regimes: Case (a) the electron current is

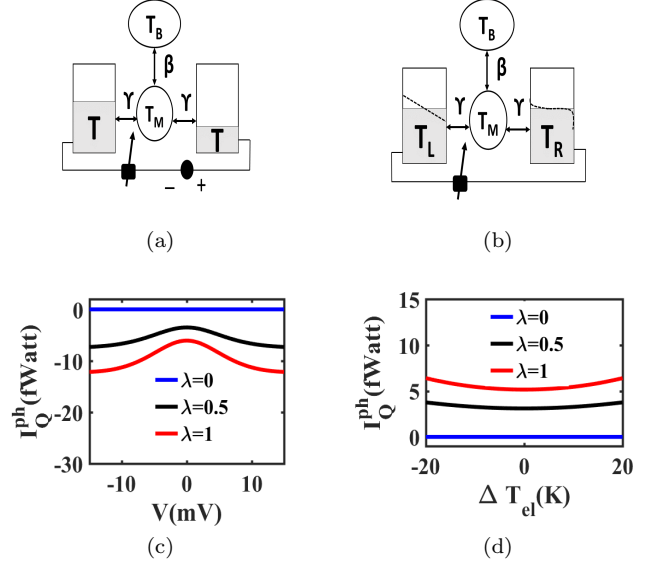


Figure 2. Electron induced phonon transport at zero phonon temperature gradient. Modified setups in two operating limits: (a) Current is driven by a voltage bias when $\Delta T_{el} = 0$. (b) Current is driven set up by an electronic temperature bias when $V = 0$. (c) Variation of I_Q^{ph} with voltage for different λ in Case (a). (d) Variation of I_Q^{ph} with ΔT_{el} for different λ in Case (b). This figure establishes that V and ΔT_{el} decide the direction of I_Q^{ph} and λ works like a phonon switch.

driven by a voltage bias when ΔT_{el} ($\Delta T_{el} = T_L - T_R$) is zero and Case (b) the electron current is set up by an electronic temperature gradient ($\Delta T_{el} = T_L - T_R \neq 0$) at zero voltage. Each case operates at zero ΔT_{ph} to ensure that only electron current influences the phonon distribution. To put things simple, reservoirs H and C are merged to a single reservoir B with temperature T_B and relaxation rate β . The modified setups in Case (a) and (b) are depicted in Fig. 2(a) and 2(b) respectively. In each operating point, the direction of phonon current is decided by the gradient between T_B and dot temperature T_M .

The preceding section established that I_{ph}^Q vanishes at $\lambda = 0$. As we turn on a finite λ , the magnitude of I_{ph}^Q increases with voltage and ΔT_{el} . Both Case (a) and (b) observe this via Fig. 2(c) and 2(d) respectively. However, we find that the direction of I_{ph}^Q is opposite in these cases. Figure 2(c) notes that in Case (a), the dot phonons relax to the reservoir and the magnitude of I_{ph}^Q increases in the negative direction. On the other way, Fig. 2(d) shows that in Case (b), the dot becomes phonon deficient and the reservoir pumps phonons into the dot. This clearly indicates that λ acts like a phonon switch whereas voltage and ΔT_{el} control the direction of I_{ph}^Q . These results can be utilized in the design of thermal transistors and rectifiers which aim to implement digital logic by modulating the heat current.

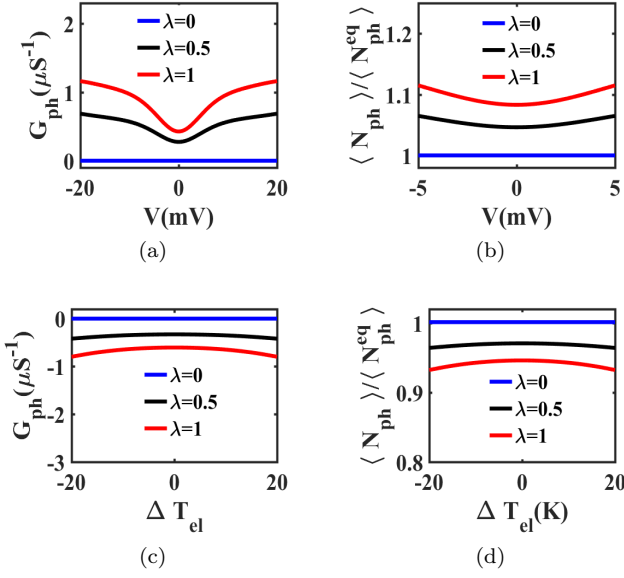


Figure 3. Study of electron induced phonon generation and absorption at finite electron-phonon interaction. (a) Variation of G_{ph} with voltage for different λ in Case (a). (b) Positive deviation of $\langle N_{ph}^{eq} \rangle$ from $\langle N_{ph}^{eq} \rangle$ as voltage increases for finite λ in Case (a). The magnitude of phonon current increases with voltage when λ is non-zero (c) Variation of G_{ph} as a function of ΔT_{el} for different λ in Case (b). (d) Negative deviation of $\langle N_{ph}^{eq} \rangle$ from the level of $\langle N_{ph}^{eq} \rangle$ as ΔT_{el} increases for non-zero λ in Case (b). We infer that in Case (a) phonons accumulate in the dot and in Case (b) phonons get absorbed and explain opposite polarity of phonon current in the two cases.

The anomaly in the direction of I_{Ph}^Q can be explained by studying the phonon generation rate (G_{ph}) in Case (a) and (b). Figure 3(a) notes that in Case (a), G_{ph} is positive and rises with voltage when λ is finite. Hence, phonons accumulate in the dot as $\langle N_{ph} \rangle$ exceeds $\langle N_{ph}^{eq} \rangle$. The voltage response of $\langle N_{ph} \rangle$ is presented in Fig. 3(b). In contrast, Fig. 3(c) observes that in Case (b), G_{ph} becomes negative and falls with ΔT_{el} when λ is non-zero. Hence the rise of ΔT_{el} facilitates phonon absorption and $\langle N_{ph} \rangle$ falls below the level of $\langle N_{ph}^{eq} \rangle$ as depicted in Fig. 3(d). As a result in Case(b), reservoirs pump phonons into the dot.

One should note that the variation of I_{ph}^Q with voltage and ΔT_{el} takes place in a non-linear fashion. Now it is essential to test the features of I_{ph}^Q in the linear regime. From the fundamental standpoint, this is imperative since Onsager's reciprocity should be validated in the linear regime. Figure 4(a) depicts that in Case (a), the

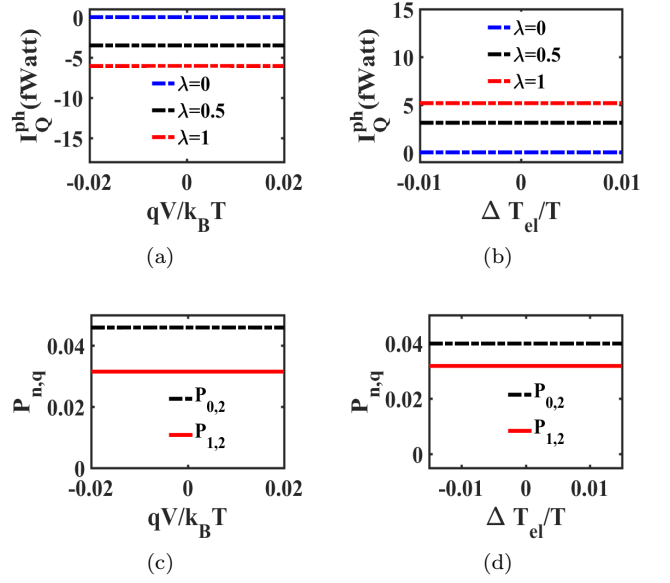


Figure 4. Linear response of I_Q^{ph} . (a) Variation of I_Q^{ph} with voltage in the linear regime for different λ in Case (a). (b) Variation of I_Q^{ph} with ΔT_{el} in the linear regime for different λ in Case (b). (c) Variation of $P_{n,q}$ with linear voltage in Case (a) at non-zero λ ($\lambda = 0.5$). (d) Variation of $P_{n,q}$ with linear range of electronic temperature bias in Case (b) at non-zero λ ($\lambda = 0.5$). This figure notes that in the linear regime the probabilities of the states $|n, q\rangle$ remain constant and consequently I_Q^{ph} show no variation with voltage or ΔT_{el} .

phonon heat current does not vary with voltage in the linear limit ($qV \ll k_B T$). Similarly, Fig.4(b) shows that in Case (b), I_{Ph}^Q does not change with ΔT_{el} in the linear range ($\Delta T_{el} \ll T$). To explore the linear response of I_Q^{ph} , we test the nature of many body electron-phonon probabilities $P_{n,q}$ of the states $|n, q\rangle$ in Case (a) and (b), when λ is non-zero. Figure.4(c) presents that in Case (a), $P_{n,q}$ does not vary with voltage. Similarly, Fig.4(d) depicts that in Case (b), $P_{n,q}$ remains constant with ΔT_{el} . Hence, in the linear regime, the average population of phonons in the dot ($\langle N_{ph} \rangle = \sum_{n,q} q P_{n,q}$)

remains unaltered and I_{Ph}^Q remains constant as dictated in (15). This implies that the electron and phonon transport are uncoupled in the linear regime.

After the discussion of linear response of I_Q^{ph} , it is essential to examine the inter-relation of electron current I and the phonon temperature gradient ($\Delta T_{ph} = T_H - T_C$). In this course, first we set ΔT_{el} at zero and test the variation of I as a function of voltage and ΔT_{ph} . Figure.5(a) and 5(b) depict the color variation of I as a function of V and ΔT_{ph} for $\lambda = 0$ and $\lambda = 0.5$ respectively. It is observed that even in the non-linear regime, I shows no

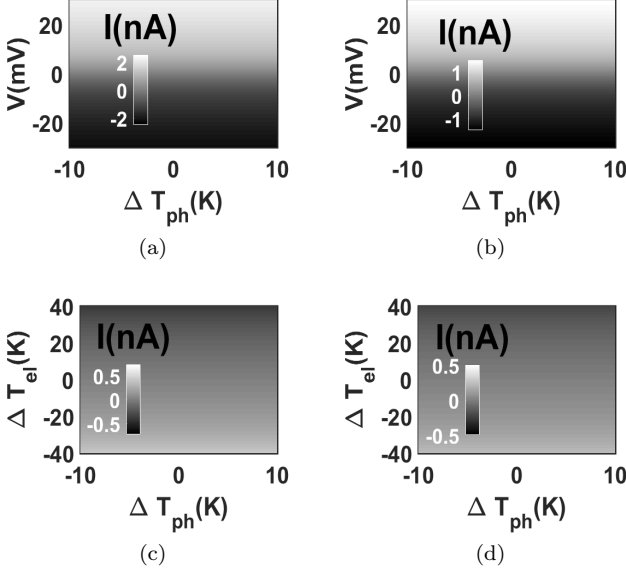


Figure 5. Test of the inter-dependence of I and ΔT_{ph} . Color variation of I as a function of ΔT_{ph} and V for (a) $\lambda = 0$ and (b) $\lambda = 0.5$ when $\Delta T_{el} = 0$. Color variation of I as a function of ΔT_{ph} and ΔT_{el} for (c) $\lambda = 0$ and (d) $\lambda = 0.5$ at zero voltage. It implies that in our setup I can not be stimulated by ΔT_{ph} even in the non-linear regime.

dependence on ΔT_{ph} . Next, we study the variation of I with ΔT_{el} and ΔT_{ph} at zero voltage. The color variation of I as a function of ΔT_{el} and ΔT_{ph} is depicted in Fig.5(c) and 5(d) for $\lambda = 0$ and $\lambda = 0.5$ respectively. Here also, we notice that I shows no dependence on ΔT_{ph} . This result is consistent with the previous report⁷¹ which demonstrated why I can not be stimulated by ΔT_{ph} in quantum dot based devices with a single phonon mode. In the linear regime, several charge and heat currents I, I_Q^{el} and I_Q^{ph} are related to voltage and various temperature gradient $V, \Delta T_{el}$ and ΔT_{ph} by the Onsager's matrix, such that

$$\begin{bmatrix} \frac{I}{q} \\ \frac{I_Q^{el}}{k_B T} \\ \frac{I_Q^{ph}}{k_B T} \end{bmatrix} = \begin{bmatrix} L_{11} & L_{12} & L_{13} \\ L_{21} & L_{22} & L_{23} \\ L_{31} & L_{32} & L_{33} \end{bmatrix} \begin{bmatrix} qV \\ k_B \Delta T_{el} \\ k_B \Delta T_{ph} \end{bmatrix}.$$

In the present scenario, we find that $L_{13} = L_{31} = 0$ and $L_{23} = L_{32} = 0$. It confirms that Onsager's reciprocity is obeyed. Now the dependence of I_Q^{ph} on the voltage and ΔT_{el} , immediately hints at the concept of a novel thermal conductivity coefficient which is different from the conventional electronic thermal conductivity. We will elaborate on it in the next subsection.

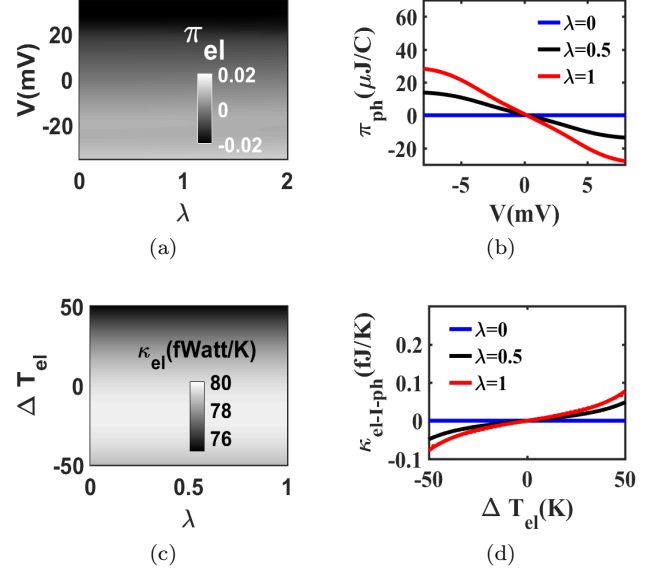


Figure 6. Phonon Peltier and electron-assisted phonon thermal conductivity coefficients. (a) Color variation of electronic Peltier coefficient π_{el} as a function of λ and V . (b) Variation of the phonon Peltier coefficient as a function of voltage for different λ . (c) Color variation of electronic thermal conductivity κ_{el} as a function of λ and ΔT_{el} . (d) Variation of $\kappa_{el}-I_{ph}$ as a function of ΔT_{el} for different λ . We infer from this figure that π_{el} and κ_{el} are independent of λ although π_{ph} and $\kappa_{el}-I_{ph}$ are strong functions of λ .

B. Non-linear phonon Peltier and electron-induced phonon thermal conductivity

The conventional electronic Peltier coefficient is defined as $\pi_{el} = \frac{dI_Q^{el}}{dI}$, when there is no electronic temperature gradient ($\Delta T_{el} = 0$). In analogy with the electronic Peltier coefficient, our previous work⁵³ has introduced the phonon Peltier coefficient as $\pi_{ph} = \frac{dI_Q^{ph}}{dI}$. In this subsection, we draw a comparative study between the two Peltier co-efficients.

Both Peltier coefficients are computed in the differential form to avoid the singularity at the short-circuit point ($V = 0$). First, we plot the color variation of π_{el} as a function of voltage and λ in Fig.6(a). It shows that π_{el} varies with voltage but remains completely independent of λ . It implies that in the absence of an electronic temperature gradient, the ratio of the electronic heat current I_Q^{el} and the charge current does not vary λ . In contrast, Fig.6(b) notes that π_{ph} is a joint function of voltage and λ . π_{ph} vanishes when λ is zero and it varies linearly with the voltage as we switch on a finite λ . Earlier Fig.2(a) showed that the magnitude of I_Q^{ph} increases with λ and Fig.5 showed that the magnitude of I falls with λ at fixed voltage. Therefore, the absolute magnitude of π_{ph} increases with λ as shown in Fig.6(b). Since I_Q^{ph} varies with voltage only in the non-linear regime, we mention

the phonon Peltier co-efficient (π_{ph}) as *non-linear phonon Peltier coefficient*.

The concept of π_{ph} was manifested since voltage bias stimulates and modulates I_Q^{ph} , when ΔT_{el} is zero. We have already observed that, I_Q^{ph} is a joint function of V and ΔT_{el} . This motivates us to propose a new thermal conductivity coefficient $\kappa_{el-I-ph}$, which is different from the conventional electronic thermal conductivity κ_{el} . Both thermal conductivity coefficients κ_{el} and $\kappa_{el-I-ph}$ are defined as,

$$\kappa_{el} = - \left. \frac{\partial I_Q^{el}}{\partial \Delta T_{el}} \right|_{I=0},$$

$$\kappa_{el-I-ph} = - \left. \frac{\partial I_Q^{ph}}{\partial \Delta T_{el}} \right|_{I=0}.$$

The color plot shown in Fig.6(c), depicts that κ_{el} remains constant with λ and shows minor variation with ΔT_{el} . On the other hand, Fig.6(d) notes that the absolute magnitude of $\kappa_{el-I-ph}$ increases with both λ and ΔT_{el} . At constant λ , the open-circuit voltage of the device increases with the increase of ΔT_{el} . On the other hand, the magnitude of I_Q^{ph} increases with the voltage bias as shown in Fig.2(a). Therefore, the absolute magnitude of $\kappa_{el-I-ph}$ rises with ΔT_{el} as shown in Fig.6(d). Therefore, the absolute magnitude of $\kappa_{el-I-ph}$ rises with ΔT_{el} . Since I_Q^{ph} varies with voltage and ΔT_{el} only in the non-linear regime, we mention $\kappa_{el-I-ph}$, as the *non-linear electron assisted phonon thermal conductivity*.

C. Engineering of I_Q^{ph} and I_Q^{el} by varying reservoir temperature

It is evident from (7),(8) and (12) that I_Q^{ph} can be controlled by differing the temperature (T_B) of the reservoir from the temperature of the electronic contacts ($T_{L(R)}$). In this subsection, we demonstrate the engineering of I_Q^{ph} in two situations: Case (HR) where, the reservoir is hotter than the contacts ($T_B = T_{BH} > T_{L(R)}$) and Case (CR) where, the reservoir is colder than the contacts ($T_B = T_{BC} < T_{L(R)}$). First, we illustrate these cases in the limit of Case (a) where I_Q^{ph} is controlled by driving the voltage bias at zero electronic temperature gradient ($\Delta T_{el} = 0$).

We present the setups in Case (HR) and (CR) in Fig.7(a). Figure 7(b) plots the voltage response of I_Q^{ph} in Case (HR). In this case, I_Q^{ph} flows from the dot to the

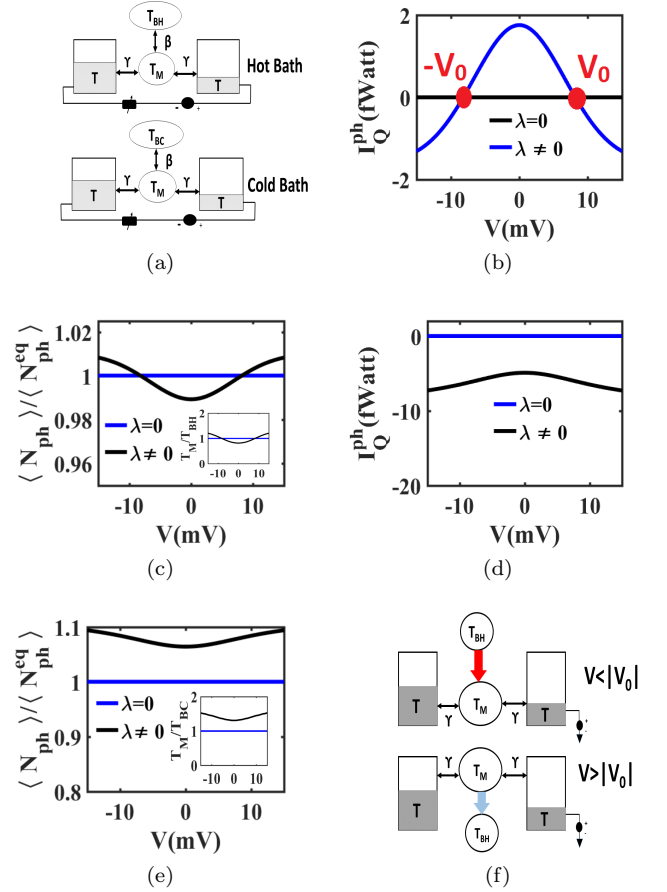


Figure 7. Control of I_Q^{ph} by voltage bias in Case (a), when $\Delta T_{el} = 0$. Two situations are considered: Case (HR) when the reservoir is hotter than the electronic contacts ($T_L = T_R = 100$ K, $T_B = T_{BH} = 150$ K) and Case (CR) when the reservoir is colder than the electronic contacts ($T_L = T_R = 150$ K, $T_B = T_{BC} = 100$ K). (a) The modified device diagrams in the two cases. (b) Voltage Variation of I_Q^{ph} for $\lambda = 0$ and $\lambda \neq 0$ in Case (HR). (c) Voltage variation of $\langle N_{ph} \rangle$ in Case (HR). Inset shows the variation of dot temperature T_M with voltage. (d) Voltage variation of I_Q^{ph} for $\lambda = 0$ and $\lambda \neq 0$ in Case (CR). (e) Voltage variation of $\langle N_{ph} \rangle$ with voltage in Case (CR). Inset shows the variation of T_M with voltage. (f) The schematic of I_Q^{ph} for Case (HR). This figure shows that in Case (a), the polarity of I_Q^{PH} can be reversed by driving the voltage in Case (HR).

reservoir in the low voltage range but reverses its polarity at $|V| = V_0$, when λ is non-zero. This non-trivial phenomenon can be explained by studying the voltage variation of $\langle N_{ph}^{eq} \rangle$ depicted in Fig.7(c). As we increase the voltage, phonons accumulate in the dot and at $V = |V_0|$, the average phonon number in the dot exceeds the equilibrium phonon number $\langle N_{ph}^{eq} \rangle$ of the reservoir. Hence, the polarity of I_Q^{ph} is flipped. However, Fig.7(d) captures no such non-trivial polarity reversal of I_Q^{ph} in Case (CR). In this case, Fig.7(e) notes that $\langle N_{ph} \rangle$ is always higher

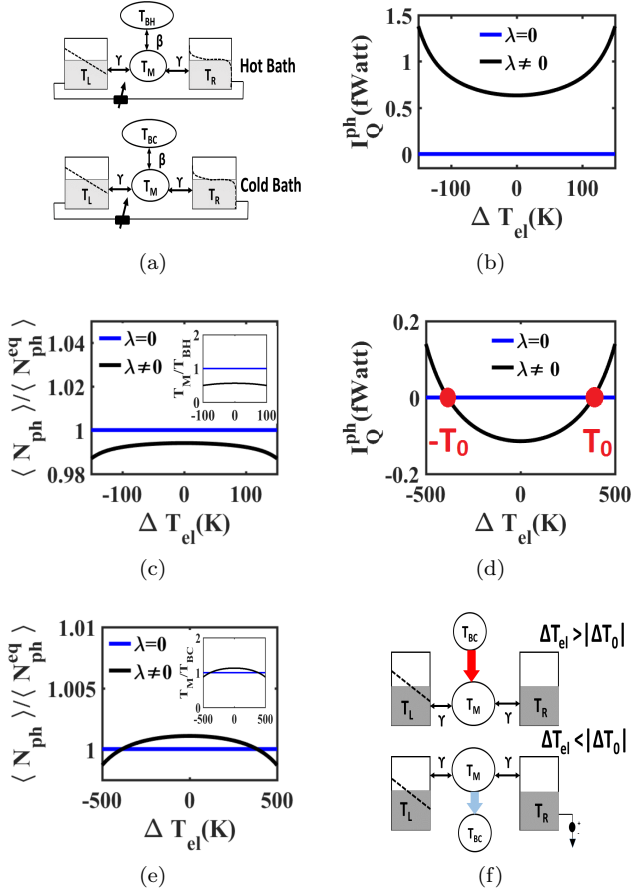


Figure 8. Control of I_Q^{ph} by driving ΔT_{el} , at $V = 0$. Two cases are considered: Case (HR) when the reservoir is hotter than the electronic contacts ($T_H = T_C = T_{BH} = 300K > T_L = T_R = 100K$) and Case (CR) Cold Bath: when the reservoir is colder than the electronic contacts ($T_H = T_C = T_{BC} = 250K < T_L = T_R = 350K$). (a) The modified device schematics in two cases. (b) Variation of I_Q^{ph} as a function of ΔT_{el} for $\lambda = 0$ and $\lambda \neq 0$ for Case (HR). (c) Variation of $\langle N_{ph} \rangle$ with ΔT_{el} in Case (HR). Inset shows the variation of T_M with ΔT_{el} in the same case. (d) Variation of I_Q^{ph} with ΔT_{el} for $\lambda = 0$ and $\lambda \neq 0$. (e) Variation of $\langle N_{ph} \rangle$ with ΔT_{el} . Inset shows the variation of T_M with ΔT_{el} in the same case. (f) The schematic of I_Q^{ph} in Case (CR). This figure infers that the schematic of that in Case (b), the polarity of I_Q^{ph} can be flipped by driving ΔT_{el} in Case (CR).

than the mark of $\langle N_{ph}^{eq} \rangle$ and I_Q^{ph} is directed from the dot to the cold reservoir. The voltage variation of $\langle N_{ph} \rangle$ presented in Fig.7(c) and 7(e) is consistent with the voltage variation of the dot temperature T_M shown in their respective insets. It is interesting to observe that the electron current emanating from electronic contacts can pump phonons into the hotter reservoir. This is a type of counter-intuitive heating of a hot reservoir. Figure 7(f) depicts the schematic of counter-intuitive heating in Case (HR).

An opposite response of I_Q^{ph} is observed when we analyze Case (HR) and (CR) in the limit of Case (b) where we drive the electronic temperature gradient at zero voltage. Figure 8(a) depicts the modified device schematics in Case (HR) and (CR). Figure.8(b) plots the variation of I_Q^{ph} with ΔT_{el} in the Case (HR) for $\lambda = 0$ and $\lambda \neq 0$. In this case, we note no non-triviality in the direction of I_Q^{ph} and reservoir pumps phonons into the dot for all values of ΔT_{el} . Fig.8(c) shows that in this case, $\langle N_{ph} \rangle$ is always lower than the level of $\langle N_{ph}^{eq} \rangle$ and I_Q^{ph} does not flip its polarity. In contrast, Fig.8(d) depicts that in Case (CR), I_Q^{ph} reverses its direction at $\Delta T_{el} = |T_0|$ for non-zero λ and cold reservoir pumps phonons into the dot. As explained earlier, the increase of ΔT_{el} enhances the absorption of phonons and the average phonon number in the dot falls below the level of at $\Delta T_{el} = |T_0|$. This phenomenon is explained with the help of Fig.8(e). The ΔT_{el} variation of $\langle N_{ph} \rangle$ presented in Fig.8(c) and 8(e) is consistent with the ΔT_{el} variation of the dot temperature T_M shown in their respective insets. Therefore, this case observes a counter-intuitive cooling of a cold reservoir. Figure 8(f) depicts the schematic of counter-intuitive cooling in the Case (CR).

Finally, we elaborate on the engineering of the electronic heat current (I_Q^{el}) in Case (HR) and (CR). In this context we rename I_Q^{el} associated with the contacts L and R as I_{QL}^{el} and I_{QR}^{el} respectively. Figure 9(a) and 9(b) depict the voltage variation of I_{QL}^{el} and I_{QR}^{el} for different values of λ in Case (HR). We observe that both I_{QL}^{el} and I_{QR}^{el} vanishes when $\lambda = 0$. When λ is non-zero, both I_{QL}^{el} and I_{QR}^{el} becomes finite and they disperse uniformly into the contacts even at the short-circuit point ($V = 0$). At $\lambda \neq 0$, the Hot Bath push phonons into the dot and the excess heat flows away into the contacts in the form of I_Q^{el} . Similarly Fig.9(c) and 9(d) explain the same phenomenon in Case (CR). In this case, the Cold Bath extracts phonons out of the dot and I_Q^{el} flows from the contacts to the dot. The whole scenario is pictorially presented in Fig.9(e). It is intriguing to notice that I_Q^{el} can be stimulated by varying the temperature of phonon reservoir even at the short circuit point $V = 0$, where the effective electron flow vanishes (i.e $I = 0$). Now if the contact L is strongly coupled to the dot as compared to the contact R , (i.e $\gamma_L \gg \gamma_R$), I_Q^{el} is dragged out from (or pushed into) the dot by the contact L . Fig.9(f) and 9(g) plot the small voltage response of I_{QL}^{el} and I_{QR}^{el} for non-zero λ in Case (HR) and (CR) respectively. They show that the hotter (colder) reservoir can selectively heat up (or cool down) L even when $V = 0$ as shown in the schematic presented in Fig.9(h). Therefore, the temperature of phonon reservoir plays a major role in the stimulation and control of the electronic and phonon heat current in the dot. We believe that this intriguing physics can be implemented in the design of thermal transistor or thermal logic devices.

IV. CONCLUSION

The anomalous behavior of phonon transport due to finite electron-phonon interaction was investigated using an *Anderson-Holstein* based dissipative quantum dot setup in two relevant cases: (a) electron flow stimulated by a voltage bias in the absence of an electronic temperature gradient and (b) electron flow driven

by the electronic temperature gradient at zero voltage. We explained the observed cumulative effects of voltage and electronic temperature gradients on the non-linear phonon currents, using a new transport coefficient termed as *electron induced phonon thermal conductivity*. It was demonstrated that under suitable operating conditions in Case (a) the dot pumped in phonons into the hotter phonon reservoirs and in Case (b) the dot extracted phonons out of the colder phonon reservoirs. Finally, we elaborated how the non-linear electronic heat current was stimulated and controlled by engineering the temperature of the phonon reservoirs coupled to the dot.

-
- * bm@ee.iitb.ac.in
- ¹ F. Giustino, Rev. Mod. Phys. **89**, 015003 (2017).
 - ² A. Lanzara, P. V. Bogdanov, X. J. Zhou, S. A. Kellar, D. L. Feng, E. D. Lu, T. Yoshida, H. Eisaki, A. Fujimori, K. Kishio, et al., Nature **412**, 510 (2001).
 - ³ S. P. Walborn, P. H. Souto Ribeiro, L. Davidovich, F. Mintert, and A. Buchleitner, Nature **440**, 1170 (2006).
 - ⁴ J. Lee, K. Fujita, K. McElroy, J. A. Slezak, Y. Wang, M. and Aiura, H. Bando, M. Ishikado, T. Masui, J.-X. Zhu, A. V. Balatsky, et al., Nature **442**, 546 (2006).
 - ⁵ I.-P. Hong, C. Brun, F. m. c. Patthey, I. Y. Sklyadneva, X. Zubizarreta, R. Heid, V. M. Silkin, P. M. Echenique, K. P. Bohnen, E. V. Chulkov, et al., Phys. Rev. B **80** (2009).
 - ⁶ M. Bianchi, E. D. L. Rienks, S. Lizzit, A. Baraldi, R. Balog, L. Hornekær, and P. Hofmann, Phys. Rev. B **81**, 041403 (2010).
 - ⁷ T. R. Hartke, Y.-Y. Liu, M. J. Gullans, and J. R. Petta, Phys. Rev. Lett. **120**, 097701 (2018).
 - ⁸ T. Frey, P. J. Leek, M. Beck, A. Blais, T. Ihn, K. Ensslin, and A. Wallraff, Phys. Rev. Lett. **108**, 046807 (2012).
 - ⁹ N. Ares, T. Pei, A. Mavalankar, M. Mergenthaler, J. H. Warner, G. A. D. Briggs, and E. A. Laird, Phys. Rev. Lett. **117**, 170801 (2016).
 - ¹⁰ J.-Y. Park, S. Rosenblatt, Y. Yaish, V. Sazonova, H. Üstünel, S. Braig, T. A. Arias, P. W. Brouwer, and P. L. McEuen, Nano Letters **4**, 193 (2004).
 - ¹¹ E. A. Laird, F. Pei, W. Tang, G. A. Steele, and L. P. Kouwenhoven, Nano Letters **12**, 517 (2012).
 - ¹² A. Javey, J. Guo, Q. Wang, M. Lundstrom, and H. Dai, Nature **424**, 654 (2003).
 - ¹³ L. H. Yu, Z. K. Keane, J. W. Ciszek, L. Cheng, M. P. Stewart, J. M. Tour, and D. Natelson, Phys. Rev. Lett. **93**, 266802 (2004).
 - ¹⁴ D. Rakhmilevitch, R. Korytár, A. Bagrets, F. Evers, and O. Tal, Phys. Rev. Lett. **113**, 236603 (2014).
 - ¹⁵ D. R. Ward, D. A. Corley, J. M. Tour, and D. Natelson, Nature Nanotechnology **6**, 33 (2010).
 - ¹⁶ Z. Ioffe, T. Shamai, A. Ophir, G. Noy, I. Yutsis, K. Kfir, O. Cheshnovsky, and Y. Selzer, Nature Nanotechnology **3**, 727 (2008).
 - ¹⁷ A. Benyamini, A. Hamo, S. Kusminskiy, F. V. Oppen, and S. Ilani, Nat. Phys. **10**, 151 (2014).
 - ¹⁸ R. Härtle and M. Thoss, Phys. Rev. B **83**, 115414 (2011).
 - ¹⁹ M. Leijnse, M. R. Wegewijs, and K. Flensberg, Phys. Rev. B **82**, 045412 (2010).
 - ²⁰ M. Galperin, M. A. Ratner, and A. Nitzan, J. Chem. Phys. **121**, 11965 (2004).
 - ²¹ M. Galperin, A. Nitzan, and M. A. Ratner, Phys. Rev. B **75**, 155312 (2007).
 - ²² B. De and B. Muralidharan, Phys. Rev. B **94**, 165416 (2016).
 - ²³ B. K. Agarwalla, J.-H. Jiang, and D. Segal, Phys. Rev. B **92**, 245418 (2015).
 - ²⁴ L. Arrachea, N. Bode, and F. von Oppen, Phys. Rev. B **90**, 125450 (2014).
 - ²⁵ B. Sothmann, R. Sánchez, and A. N. Jordan, Nanotechnology **26**, 32001 (2014).
 - ²⁶ L. Siddiqui, A. W. Ghosh, and S. Datta, Phys. Rev. B p. 085433 (2006).
 - ²⁷ a. Mitra, I. Aleiner, and a. J. Millis, Phys. Rev. B **69**, 245302 (2004).
 - ²⁸ Y. Kim, W. Jeong, K. Kim, W. Lee, and P. Reddy, Nat. Nanotechnol. **9**, 881 (2014).
 - ²⁹ P. Reddy, S.-Y. Jang, R. A. Segalman, and A. Majumdar, Science **315**, 1568 (2007).
 - ³⁰ J. Roßnagel, S. T. Dawkins, K. N. Tolazzi, O. Abah, E. Lutz, F. Schmidt-Kaler, and K. Singer, Science **352**, 325 (2016).
 - ³¹ G. A. Steele, A. K. Hüttel, B. Witkamp, M. Poot, H. B. Meerwaldt, L. P. Kouwenhoven, and H. S. J. van der Zant, Science **325**, 1103 (2009).
 - ³² B. Lassagne, Y. Tarakanov, J. Kinaret, D. Garcia-Sanchez, and A. Bachtold, Science **325**, 1107 (2009).
 - ³³ M. T. Woodside and P. L. McEuen, Science **296**, 1098 (2002).
 - ³⁴ J.-H. Jiang, M. Kulkarni, D. Segal, and Y. Imry, Phys. Rev. B **92**, 045309 (2015).
 - ³⁵ L. Wang and B. Li, Phys. Rev. Lett. **99**, 177208 (2007).
 - ³⁶ L. Wang and B. Li, Phys. Rev. Lett. **101**, 267203 (2008).
 - ³⁷ N. Li, J. Ren, L. Wang, G. Zhang, P. Hänggi, and B. Li, Rev. Mod. Phys. **84**, 1045 (2012).
 - ³⁸ K. Joulain, J. Drevillon, Y. Ezzahri, and J. Ordóñez-Miranda, Phys. Rev. Lett. **116**, 200601 (2016).
 - ³⁹ G. D. Mahan and J. O. Sofo, Proceedings of the National Academy of Sciences of the United States of America **93**, 7436 (1996).
 - ⁴⁰ B. Kubala and J. König, Phys. Rev. B **73**, 195316 (2006).
 - ⁴¹ B. Kubala, J. König, and J. Pekola, Phys. Rev. Lett. **100**, 066801 (2008).
 - ⁴² H. Park, J. Park, A. Lim, E. Anderson, A. Alivisatos, and P. McEuen, Nature **407**, 57 (2000).

- ⁴³ B. J. Leroy, S. G. Lemay, J. Kong, and C. Dekker, *Nature* **432**, 371 (2004).
- ⁴⁴ B. J. LeRoy, J. Kong, V. K. Pahilwani, C. Dekker, and S. G. Lemay, *Phys. Rev. B* **72**, 075413 (2005).
- ⁴⁵ L. H. Yu, Z. K. Keane, J. W. Ciszek, L. Cheng, M. P. Stewart, J. M. Tour, and D. Natelson, *Phys. Rev. Lett* **93**, 266802 (2004).
- ⁴⁶ S. Sapmaz, P. Jarillo-Herrero, Y. M. Blanter, C. Dekker, and H. S. J. Van Der Zant, *Phys. Rev. Lett* **96**, 026801 (2006).
- ⁴⁷ T. L. Schmidt and A. Komnik, *Phys. Rev. B* **80**, 041307 (2009).
- ⁴⁸ D. F. Urban, R. Avriller, and A. Levy Yeyati, *Phys. Rev. B* **82**, 121414 (2010).
- ⁴⁹ R. Egger and A. O. Gogolin, *Phys. Rev. B* **77**, 113405 (2008).
- ⁵⁰ R. Seoane Souto, A. L. Yeyati, A. Martín-Rodero, and R. C. Monreal, *Phys. Rev. B* **89**, 085412 (2014).
- ⁵¹ H. Ness, *Phys. Rev. B* **89**, 045409 (2014).
- ⁵² E. Y. Wilner, H. Wang, M. Thoss, and E. Rabani, *Phys. Rev. B* **89**, 205129 (2014).
- ⁵³ B. De and B. Muralidharan, *Scientific Reports* **8**, 5185 (2018).
- ⁵⁴ S. Braig and K. Flensberg, *Phys. Rev. B* **68**, 205324 (2003).
- ⁵⁵ D. Segal and A. Nitzan, *J. Chem. Phys.* **122** (2005).
- ⁵⁶ D. Segal, *Phys. Rev. B* **73**, 205415 (2006).
- ⁵⁷ D. Segal and A. Nitzan, *Phys. Rev. Lett* **94**, 034301 (2005).
- ⁵⁸ B. Muralidharan, A. W. Ghosh, and S. Datta, *Phys. Rev. B* **73**, 155410 (2006).
- ⁵⁹ B. Muralidharan and S. Datta, *Phys. Rev. B* **76**, 035432 (2007).
- ⁶⁰ C. W. J. Beenakker, *Phys. Rev. B* **44**, 1646 (1991).
- ⁶¹ B. Muralidharan and M. Grifoni, *Phys. Rev. B* **88**, 045402 (2013).
- ⁶² B. Muralidharan and M. Grifoni, *Phys. Rev. B* **85**, 155423 (2012).
- ⁶³ C. Timm, *Phys. Rev. B* **77**, 195416 (2008).
- ⁶⁴ G. Piovano, Effects of Electron-Vibron Coupling in Nano-electromechanical Systems **Phd Thesis** (2012).
- ⁶⁵ S. Braig and P. W. Brouwer, *Phys. Rev. B* **71**, 195324 (2005).
- ⁶⁶ J. König and J. Martinek, *Phys. Rev. Lett.* **90**, 166602 (2003).
- ⁶⁷ M. Braun, J. König, and J. Martinek, *Phys. Rev. B* **70**, 195345 (2004).
- ⁶⁸ J. Koch and F. Von Oppen, *Physical Review Letters* **94**, 206804 (2005).
- ⁶⁹ J. Koch, M. Semmelhack, F. Von Oppen, and A. Nitzan, *Phys. Rev. B* **73**, 155306 (2006).
- ⁷⁰ J. Koch, Quantum transport through single-molecule devices **Phd Thesis** (2006).
- ⁷¹ J.-T. Lü, J.-S. Wang, P. Hedegård, and M. Brandbyge, *Phys. Rev. B* **93**, 205404 (2016).

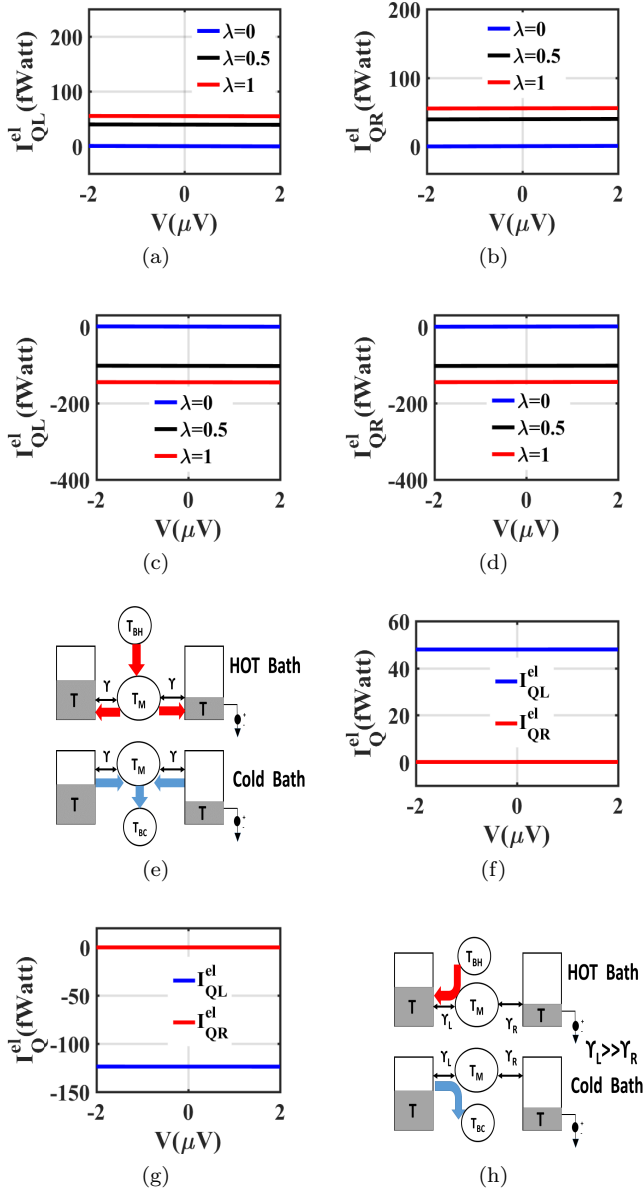


Figure 9. Study of small voltage response of electronic heat current $I_{Q L(R)}^{el}$ associated with contact $L(R)$, when $\Delta T_{el} = 0$. We consider two cases: (1) Hot Bath: $T_H = T_C > T_L = T_R$ and (2) Cold Bath: $T_H = T_C < T_L = T_R$. (a) and (b) plot the respective voltage variation of $I_{Q L}^{el}$ and $I_{Q R}^{el}$ for Hot Bath as λ varies. Similarly (c) and (d) show the respective voltage variation of $I_{Q L}^{el}$ and $I_{Q R}^{el}$ for Cold Bath as λ varies. (e) Present the schematic of $I_{Q L(R)}^{el}$ in two cases. (f) and (g) depict the voltage dependence of $I_{Q L}^{el}$, $I_{Q R}^{el}$ for non-zero λ for cases (1) and (2) respectively, when $\gamma_L \gg \gamma_R$. (h) presents the schematic for two cases given $\gamma_L \gg \gamma_R$.